
Article:
Shackleford, A.S.D., Williams, R.J., Brown, R. et al. (2 more authors) (2021) Degradation of laser sintered polyamide 12 parts due to accelerated exposure to ultraviolet radiation. Additive Manufacturing, 46. 102132. ISSN 2214-7810

https://doi.org/10.1016/j.addma.2021.102132

Additive Manufacturing 46 (2021) 102132

Contents lists available at ScienceDirect

Additive Manufacturing

journal homepage: www.elsevier.com/locate/addma

Research Paper

Degradation of Laser Sintered polyamide 12 parts due to accelerated exposure to ultraviolet radiation

Alec S.D. Shackleford [a], Rhys J. Williams [b], Ryan Brown [c,*], James R. Wingham [c], Candice Majewski [c]

[a] Radiological Physics, Sheffield Teaching Hospitals NHS Foundation Trust, Sheffield, UK
[b] Department of Natural Sciences, John Dalton Building, Manchester Metropolitan University, Manchester, UK
[c] Department of Mechanical Engineering, University of Sheffield, Sheffield, UK

ARTICLE INFO

Keywords:
Additive manufacturing
Laser Sintering
UV ageing
Polyamide 12
Positron Annihilation Lifetime Spectroscopy

ABSTRACT

Laser Sintering is an additive manufacturing technology capable of producing robust, geometrically complex polymer parts, with polyamide 12, also known as nylon-12, the most common and well understood feedstock powder. While Laser Sintering has drawn increased interest from industry for producing end-use components directly, little information is currently available regarding the effects of in-service conditions on mechanical performance. When considering applications where parts spend significant periods of time outdoors, such as the automotive sector, the effect of exposure to natural UV light is an obvious concern.

To assess their suitability for long-term outdoor applications, Laser-sintered polyamide 12 parts were subjected to up to 2 months of constant UVB radiation. UV exposure was found to cause significant yellowing of the parts, evidenced by their reflectance of blue light decreasing continually as exposure time was increased beyond 24 h. Results from UV/visible spectroscopy demonstrated an increase in UV absorbance with exposure time, attributed to increasing carbonyl concentration. Similarly, X-ray photo-electron spectroscopy showed increases in surface oxygen concentration proportional to UV exposure, with changes to the O 1s and C 1s environments after 2 months of exposure consistent with the generation of new carboxylic acid groups. Photo-degradation led to substantial decreases in both Ultimate Tensile Strength and Elongation at Break, with the deterioration first becoming appreciable between one and two weeks of exposure. Mono-energetic Positron Spectroscopy, a non-destructive surface analysis technique, demonstrated a correlation between these mechanical properties and free volume at the parts' surfaces. Decreases in free volume were concluded to be due to changes in the nature of the polymer crystal structure and an increase in overall crystallinity at the part surfaces after UV exposure, identified using DSC. Overall, it was concluded that UV exposure causes significant deterioration of Laser-sintered polyamide 12 parts and this should be mitigated against prior to use in long-term outdoor applications.

1. Introduction

Additive Manufacturing (AM) has seen increasing uptake by industry over recent years, with an estimated $1.4 billion spent on final part production using AM in 2019 [1]. This is a consequence of the benefits afforded by AM, such as increased geometric freedom and reduced material waste, combined with improving machine reliability and speed [2,3]. For polymers, Powder Bed Fusion (PBF) is considered well suited for the manufacture of end-use parts, largely due to its ability to produce parts with relatively high mechanical properties without the need for support structures [4]. Of the range of PBF systems currently commercially available, Laser Sintering is the most well-established.

The Laser Sintering process produces parts by selectively scanning and sintering consecutive layers of polymeric powder using a CO_2 laser (Fig. 1), with unsintered material acting as support [5]. While the effects of processing parameters on the mechanical performance of Laser Sintered parts are well documented [6–8], the effects of in-service conditions on performance are less well understood.

Despite the range of materials available for Laser Sintering increasing in recent years, polyamide 12 remains the most commonly used, accounting for over 90% of the polymer PBF market [10]. A key factor behind the widespread use of polyamide 12 in PBF is the material's large supercooling window, which is defined as the difference between

* Corresponding author.
E-mail address: ryan.brown@sheffield.ac.uk (R. Brown).

https://doi.org/10.1016/j.addma.2021.102132
Received 13 April 2021; Received in revised form 14 June 2021; Accepted 17 June 2021
Available online 22 June 2021

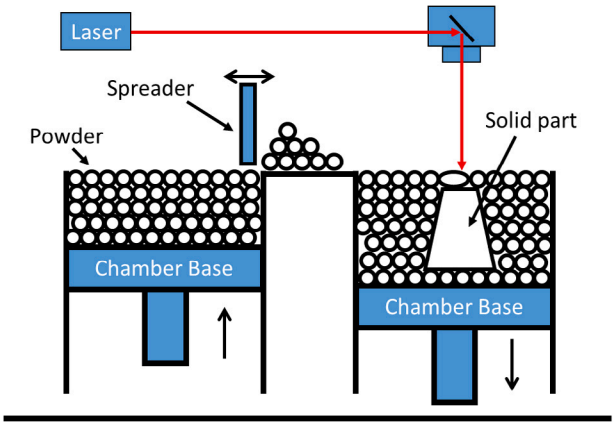

Fig. 1. Schematic of the Laser Sintering process (recreated based on a literature design [9]).

the melting and crystallisation temperatures of the powder [11]. As sintered material is required to be held within this range throughout a build to prevent crystallisation-induced shrinkage and warpage, a wider supercooling window mitigates the effects of any temperature variations across the part bed [11]. The polymer's relatively well defined onset of melting also lends itself well to Laser Sintering. This property enables the part bed to be maintained at a temperature close to the material's melting point to promote part densification after sintering, whilst limiting unwanted sintering of powder outside of the laser's scanning path which would reduce part accuracy. As a result, Laser Sintered polyamide 12 parts exhibit tensile strength comparable to injection moulding [10].

Due to its ease of processing and relatively robust mechanical properties when Laser Sintered, in addition to the polymer's chemical resistance to a variety of common solvents [12], polyamide 12 is a viable material choice for industry sectors aiming to take advantage of the benefits of Additive Manufacturing. One such sector is the automotive industry, with car manufacturers such as BMW and Ford investing in polymer AM technologies for the production of end-use parts [13,14]. With the number of Additively Manufactured polymer components found in production cars likely to increase in the coming years, understanding the effect of environmental weathering on these parts is important. Given cars spend a large portion of their service life outdoors, extended exposure to UV radiation from natural sunlight is likely to be an increasing issue.

Synthetic organic polymers, including polyamides, have long been known to undergo degradation when subjected to UV radiation [15]. This is typically initiated by the absorption of a UV photon by some impurity in the polymer to generate a free radical pair [15]. For example, in polyamides, α,β-unsaturated carbonyl impurities have been shown to be important initiators of photodegradation [16]. Reactive free radicals can then propagate through the material via a complex set of mechanisms, including hydrogen abstraction, or reaction with molecular oxygen to form hydroperoxide groups, which can in turn dissociate to propagate radicals and generate new oxygen-bearing groups on the polymer chain [15,17]. The outcomes of these processes are varying extents of cross-linking and chain scission throughout the material, including the generation of a wide variety of new functional end-groups. For example, in the case of polyamide 6-6, Caroccio et al. identified 40 unique compounds after exposure to UV using mass spectrometry, as opposed to just four in the initial material [17]. These newly-generated groups included alkyl, alkenyl, and amine groups, in addition to new ketones, aldehydes, and carboxylic acids produced by photo-oxidation (i.e. via reactions with atmospheric oxygen) [17]. It is therefore clear that exposure to UV leads to significant chemical changes within polyamide polymers.

The consequences of photo-degradation induced chemical changes on the material properties of polyamides have been studied by a variety of authors. For example, chain scission after UV exposure has been associated with a change in the crystal structure of polyamide 6 [18] and polyamide 6-6 [19]. For polyamide 6 specifically, UV exposure was also associated with decreases in the intrinsic viscosity of the polymer and chain mobility in the amorphous region [18]. Damage caused by UV exposure has also been shown to have implications for end-use applications of polyamide polymers, with Fujiwara and Zeronian demonstrating that UV exposure led to significant cracking of the surfaces of polyamide 6 filaments [20]. Furthermore, Moezzi et al. showed that UV exposure can cause a reduction in the shear modulus of polyamide 6-6 conveyor belt fabrics [21]. Exposure to UV radiation is also known to cause discolouration, specifically yellowing, of polyamides [22]. This is an obvious concern where the aesthetic properties of parts are valuable, as is often the case for automotive components. However, while it is clear that UV irradiation can cause detrimental changes to the material properties of polyamide polymers, there have been few published studies regarding the effect of UV irradiation on either the mechanical properties of polyamide 12 in general, or Laser Sintered polyamide 12 parts specifically. From the existing literature, only the effect of UV ageing on the hardness of Laser Sintered polyamide 12 parts has been investigated [23], with other long-term studies instead exploring the effect of humidity and water immersion on mechanical performance [24]. It is therefore important to establish the extent to which such parts are affected mechanically by UV exposure before they can be adopted for outdoor applications.

This research focuses on the effects of UV exposure on Laser Sintered polyamide 12 parts. Manufactured test coupons were subjected to UV radiation for varying periods of time, before Colorimetry and UV/vis reflectance spectroscopy were performed to quantify the changes in visible and UV reflectance of the parts. X-ray Photoelectron Spectroscopy (XPS) was subsequently carried out to elucidate the chemical changes within the material. Alongside the investigation into UV's effect on the aesthetic properties of Laser Sintered polyamide 12 parts, tensile testing was conducted to assess its effect on mechanical performance. Changes in tensile properties with increasing UV exposure were compared with changes in the "free volume" between polymer chains, used as an indicator of nanoscale structural changes at the part surface. This was achieved using Mono-energetic Positron Spectroscopy (MePS), a type of Positron Annihilation Lifetime Spectroscopy (PALS) whereby the size of nanopores within materials can be quantified by measuring the time taken for a positron to annihilate with an electron in the material's free volume [25]. By manipulating the energy supplied to these positrons, different implantation depths can be achieved, allowing profiling of nanoporosity as a function of depth from the surface of the material [26]. Following this, DSC was carried out to correlate changes in free volume observed by MePS with changes in the nature and extent of crystallinity at the part surface, before comparing these with results from the bulk. Overall, it was demonstrated that UV irradiation caused significant deterioration of polyamide 12 parts, with chemical changes resulting from UV exposure leading to structural changes at the polymer surface, manifesting as changes in the macroscopic mechanical properties of the parts.

2. Methodology

2.1. Laser Sintered part production

All test coupons were produced in virgin polyamide 12 (PA2200, EOS) using an EOS Formiga P100 Laser Sintering machine. A total of 32 ASTM D638 type IV tensile test bars were manufactured using machine supplier standard processing parameters for polyamide 12 (Table 1) for use in tensile testing and DSC. An equal number of 15 mm × 15 mm × 2 mm tiles were also produced for analysis using Colorimetry, UV/vis reflectance spectroscopy, XPS and MePS. Upon

Table 1
Laser Sintering machine parameters.

Parameter	Value	Units
Powder bed temperature	170	°C
Warm-up rate from room temperature	1	°C min^{-1}
Laser power	21	W
Laser scan speed	2500	mm s^{-1}
Laser scan spacing	0.25	mm
Layer height	0.1	mm

Table 2
DSC programme used to identify the peak melt temperature and crystallinity of UV irradiated Laser Sintered polyamide 12 parts.

Step number	Step details
1	Hold at 20 °C for 1 min
2	Heat from 20 °C to 250 °C at 10 °Cmin^{-1}
3	Hold at 250 °C for 1 min
4	Cool from 250 °C to 20 °C at 10 °Cmin^{-1}
5	Hold at 20 °C for 1 min

build completion, test coupons were removed from the part bed and cleaned using a combination of compressed air and glass blast media, as is standard in polymer Laser Sintering. The parts were then wrapped in aluminium foil to minimise exposure to ambient UV prior to the controlled UV exposure experiments.

2.2. Accelerated UV weathering

Artificial UV weathering was conducted using an Atlas UV Test instrument (Atlas Material Testing Solutions) fitted with eight UVB lamps (313 nm wavelength). Four tensile test bars and tiles were mounted onto aluminium plates using adhesive tape for each exposure time investigated. The UV tester was set to hold a temperature of (25 ± 3) °C and a constant UV intensity of 0.5 W m^{-2} for up to 1344 h (2 months). As a reference for how this compares to real-world conditions, 2 months in the UV tester correlates to approximately 2.86 years of exposure to the irradiance experienced on a midsummer's day in Denver, US. [27]. A set of samples were then removed at one of 12 UV exposure times: 0, 1, 2, 4, 8, 24, 48, 96, 168, 336, 672, and 1344 h. After exposure, samples were kept wrapped in aluminium foil when they were not being analysed to prevent further exposure to ambient UV.

2.3. Colorimetry

Changes in part colour due to UV exposure were measured using a PCE Instruments handheld PCE-RGB2 Colorimeter, utilising the red, green, blue (RGB) colour model to describe visible light reflectance. For each sample, 32 measurements were made at different positions, averaged and the standard error determined. RGB (red, green, blue) light intensity was recorded and a decrease in blue intensity was used as an indicator for an increase in yellowing. The instrument was calibrated using the white paper standard provided by PCE Instruments.

2.4. UV/vis reflectance spectroscopy

Changes in reflectance (and therefore absorption) of UV and visible light by the parts was measured using an Ocean Optics (USA) USB2000+ spectrometer with a bifurcated reflectance probe. The light source was a PX-2 pulsed Xenon light source (Ocean Optics, USA). The probe was placed close to and orthogonal to the sample surface. Spectra were collected using an integration time of 0.35 s, a boxcar width of 3 nm, and averaging 5 scans per measurement. The spectra were normalised by referencing to the reflectance of an Ocean Insight WS-1 Spectralon diffuse reflectance standard. MATLAB R2019a was used to apply the Kubelka–Munk model to the spectra, to subtract a constant baseline from each measurement (taken as the minimum value of $\frac{k}{s}$ for that measurement), and to integrate the resulting data over UV wavelengths.

2.5. X-ray photoelectron spectroscopy

Chemical changes arising from exposure to UV radiation were identified using a Kratos Axis Supra X-ray Photoelectron Spectrometer with a monochromatic aluminium source. As well as charge neutralisation, in order to minimise static charging of the insulating samples during measurement, conductive copper tape was used to provide a conducting path between the samples and the grounded instrument. The data was analysed using Casa XPS. The binding energy scale was calibrated by setting the C–C/C-H C 1s peak at 285.0 eV.

2.6. Tensile testing

Changes in the mechanical performance of irradiated parts were measured using a Tinius Olsen H5KS tensometer with a H500L laser extensometer. Tensile testing was carried out in accordance with ASTM D638, specifically using Type IV specimen dimensions and testing at a rate of 5(mm)min^{-1}. Cross-sectional areas used to determine ultimate tensile strength were calculated using average width and thickness measurements taken from three points along the gauge length of each test coupon.

2.7. Positron annihilation studies

Nanoscale structural changes at the part surface were investigated using the ELBE Centre's Mono Energetic Positron Spectrometer (MePS) at the Helmholtz Zentrum in Dresden-Rossendorf facility (HZDR). For each sample, implantation energies of 1-10, 12, 14, 16 and 18 keV were used to investigate potential structure changes at different depths within the parts. Each energy was converted into a mean implantation depth based on the Markov model [28,29]. Ten million counts were collected per spectrum at each energy at a rate of 100–150 kcps. Each lifetime spectrum was analysed using LTPolymers software, based on a three-component model with the parapositronium (pPs) component fixed at 0.125 ns. Full details of the MePS instrument are presented by Wagner et al. [30,31].

2.8. Differential Scanning Calorimetry (DSC)

Changes to the nature and degree of crystallinity at the surface and in the bulk of the parts were assessed using a Perkin Elmer DSC8500 Differential Scanning Calorimeter. Approximately 5 mg of material was removed from the UV exposed surface of a tensile test coupon and press sealed into an aluminium pan for testing using the programme outlined in Table 2. A second sample of the centre of the test coupon was obtained by removing the top layer of material from the unexposed surface and collecting approximately 5 mg of material from underneath. Surface and bulk samples were obtained from each of the four samples for a given UV exposure time. The peak melt temperature and specific melt enthalpy for each sample were calculated using the "Peak Area" function in Perkin Elmer's Pyris software. A temperature range was selected between which a baseline was drawn, such that the melting peak could be distinguished from the rest of the trace (Fig. 2). The melt enthalpy of each sample was then determined by dividing the area bound by the trace and baseline by the mass of the sample.

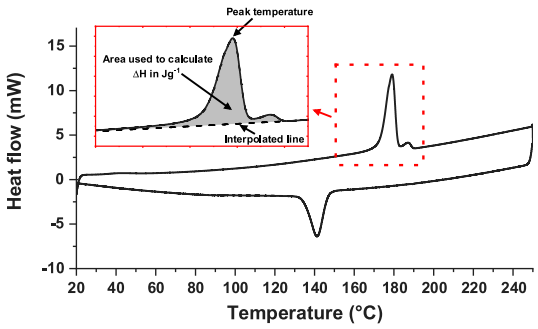

Fig. 2. An example DSC trace with the inset figure highlighting the region used to determine the specific melt enthalpy of a sample.

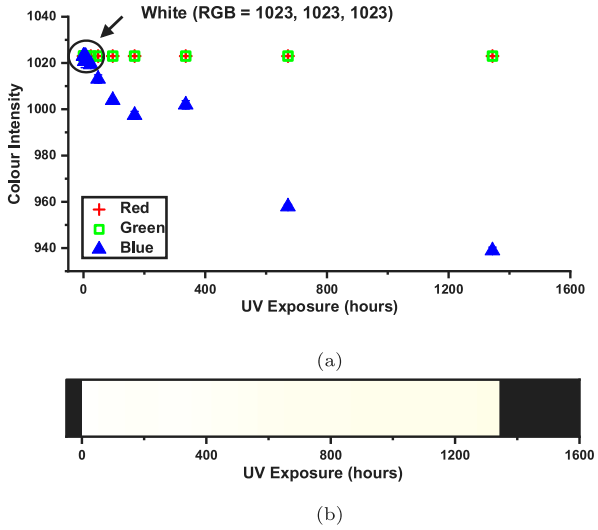

Fig. 3. (a) Red, green and blue (RGB) colour values as measured by colorimetry as a function of UV exposure time. The standard error of 32 measurements are shown but are smaller than the data point size. (b) A colour bar represents the actual colour of the parts which change from white to slightly yellow. (For interpretation of the references to colour in this figure legend, the reader is referred to the web version of this article.)

3. Results

3.1. Part discolouration

Exposure to UV radiation was found to cause a colour change which was visible to the naked eye, with parts becoming progressively more yellow in appearance as exposure time increased. This represents a deterioration in the aesthetic properties of the parts and is an important consideration for many applications.

Fig. 3 shows the RGB colour intensity (10-bit precision) of LS parts as a function of UV exposure time. A visual representation of the true part colour over time is also shown by a colour bar below the graph. Unexposed polyamide 12 parts (0 h exposure time) returned three RGB values of 1023, indicating the part was perfectly white in colour. However, after 24 h a noticeable decrease in the blue light component was observed. With the exception of the anomaly at 336 h, this continued to decrease with additional exposure to UV. The red and green components remained at a constant value of 1023 over the full range of exposure times tested.

The decrease in the reflectance of blue light, in conjunction with constant reflectance of red and green light, was consistent with the part yellowing observed by eye. In addition to demonstrating that the aesthetic properties of LS polyamide 12 parts decrease continuously upon UV exposure, this also suggested a continuous chemical change

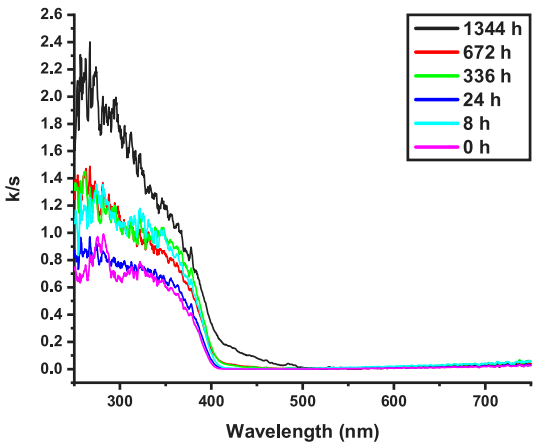

Fig. 4. A plot of $\frac{k}{s}$ calculated using Eq. (1) against wavelength for a selection of UV exposure times. Using $\frac{k}{s}$ as a proxy for absorbance, it can be concluded that increasing UV exposure time leads to an increase in the absorption of both UV and short-wavelength visible light.

at the part surface, with a greater concentration of blue-light-absorbing species being generated.

3.2. UV/vis reflectance spectroscopy

To study the colour change more precisely, and to gain information about the UV absorption of the parts, reflectance spectroscopy on the exposed surfaces was carried out over UV and visible wavelengths. In order to directly compare the concentrations of the absorbing species in the samples, the Kubelka–Munk model was applied. By assuming the samples were infinitely thick, homogeneous, and present no specular reflection (among other assumptions), the percentage reflectance, R, was used to derive an absorption coefficient (k) and scattering coefficient (s) using Eq. (1) [32]. Assuming the scattering coefficient was then constant between samples, $\frac{k}{s}$ is directly proportional to absorbance, and therefore can be used to compare the concentrations of the light absorbing species in each sample [33]. It should be noted however that Eq. (1) is only an approximation, since the samples measured here are known to violate several of these assumptions. For example, the samples are porous rather than homogeneous, and specular reflection does indeed occur from any flat particle surfaces protruding from the sample surface. Similarly, it is unknown whether the value of s is comparable for every sample. Nonetheless, the Kubelka–Munk model provides a simple means of comparing the concentrations of UV absorbing species in the samples as a function of exposure time.

$$\frac{k}{s} = \frac{(100 - R)^2}{200R} \tag{1}$$

A plot of $\frac{k}{s}$ versus wavelength is shown in Fig. 4. Total reflectance was found to not always correlate with UV exposure time; for example, the sample with 8 hours of UV exposure appeared duller than that with 24 hours of exposure. Nonetheless, in general it could be stated that additional UV exposure resulted in greater absorbance of light across the UV and visible ranges. In particular, at long UV exposure times, absorbance at the shorter wavelengths of the visible range demonstrated a pronounced increase, indicating that the samples had begun to absorb blue light. This was consistent with the colour changes seen in Section 3.1. While noise makes it difficult to decipher individual peaks and peak positions, the UV absorption was consistent with that of carbonyl (C=O) bearing species present in the pure polymer [34,35], and known to be generated during UV-initiated photo-oxidation of polyamide polymers [17,36].

The area under $\frac{k}{s}$ versus wavelength was determined for each sample by numerically integrating between 250 nm and 400 nm, serving

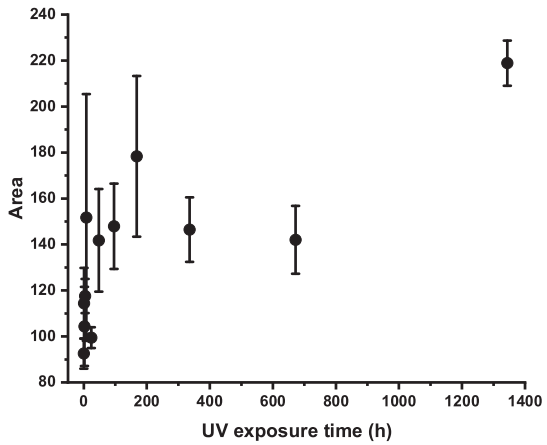

Fig. 5. The areas under plots of $\frac{A}{\lambda}$ against wavelength (between 250 nm and 400 nm) for each sample versus UV exposure time. These areas are used as a proxy for total UV absorbance by the samples. There is a positive correlation between UV absorbance and UV exposure time, which suggests a continuous increase in the concentration of carbonyl species as UV weathering proceeds. The error bars are standard deviation.

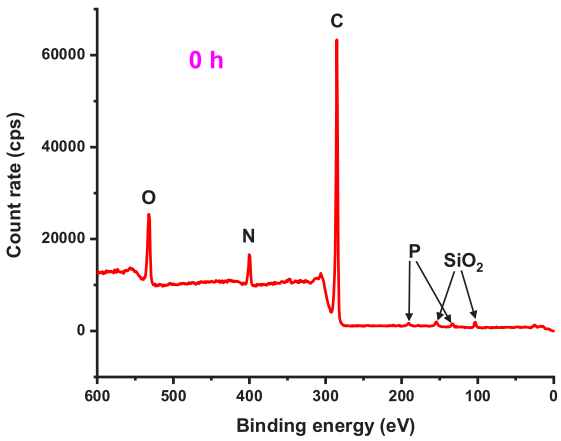

Fig. 6. An XPS survey scan of a polyamide 12 that had not been subjected to UV weathering. In addition to O, N, and C, there are also traces of Si and P in the sample.

as a proxy for the total absorbance of the samples over this wavelength range. These areas are plotted against UV exposure time in Fig. 5. Despite an apparent trend, it cannot be stated that there is a clearly defined relationship between UV exposure time and UV absorbance. This is due to the fact that it is unknown how comparable the reflective surfaces of each sample were. In the case of Fig. 5, it is unknown if the relatively low absorbances of the samples at 336 and 672 h of UV exposure were a consequence of the carbonyl concentration truly not increasing over these exposure times, or a result of the samples' surfaces back-scattering light to a greater extent. Nonetheless, there is clearly a positive correlation between UV exposure time and the absorbance of the samples in the UV region. This suggests that UV absorbing carbonyl species continuously increase in concentration in the polyamide 12 samples as UV weathering progresses.

3.3. X-ray photoelectron spectroscopy

Having identified changes in absorption across UV and visible wavelengths consistent with the presence of additional carbonyl species, X-ray photoelectron spectroscopy (XPS) was used to study these chemical changes in more detail. Fig. 6 shows a low resolution survey scan of a polyamide 12 sample exposed to no UV weathering. As can be seen from the spectra, the sample contains O, N, and C, as expected, but small peaks corresponding to P and Si (as part of silica, SiO_2) were also found. These were speculated to be included in the polyamide 12 powder as antioxidants and flow agents, respectively. Both elements were present in such small quantities that the compounds that they correspond to were assumed to have an insignificant contribution to the intensities of the O, N, or C peaks.

Fig. 7 shows high resolution scans of the O 1s, N 1s, and C 1s environments in the unexposed sample. The positions of the fitted peak centres are given in Table 3, and can be understood with regards to the polymer's chemical structure by reference to Fig. 8.

The O 1s region required two peaks for acceptable fitting, which was unexpected based on the structure of polyamide 12 (where there is only one O environment). This also contrasted with previously reported XPS data for the similar polymer, polyamide 6, where one peak could be adequately fitted to the spectra [37]. The peak at 532.9 eV (B) was consistent with the presence of carboxylic acid groups [38], and so was concluded to arise from the presence of carboxylic acid end groups on the polymer, as well as traces of impurities, such as unreacted monomer, which have been found to be present in similar grades of polyamide 12 powder used for Additive Manufacturing [39]. The peak

Table 3
Peak positions on the O 1s, N 1s, and C 1s environments of an unexposed polyamide 12 sample.

Element	Peak	Binding energy /eV	Assignment
O	B	532.9	O=C–O–H
	A	531.3	O=C
N	n/a	399.8	O=C–N
C	4	288.5	O=C–O
	3	287.6	O=C–N
	2	286.0	O=C–N–C + C–C=O
	1	285.0	CH_2

centred at 531.3 eV (A) was consistent with the carbonyl oxygen found for other polyamide polymers [38].

The N 1s environment could be fitted with a single peak centred at 399.8 eV, which was consistent with previous results for polyamide polymers [37].

The C 1s region was best fitted with four peaks corresponding to: nine C in the alkyl chain (Peak 1), a combination of the two C adjacent to the amide group (Peak 2), the C in the amide group (Peak 3), and the C in carboxylic acid end groups/impurities (Peak 4). This was in contrast to previous literature where the two C adjacent to the amide group were fitted separately to one another [37,40]. However, in this case, fitting these two peaks separately was found to be unsatisfactory. Furthermore, the peaks for the combined amide-adjacent C (Peak 2) and the alkyl chain (Peak 1) produced an intensity ratio of approximately 2:9, which is what would be expected from the structure of polyamide 12. The presence of two distinct carbonyl C 1s environments for untreated polyamide 12 (Peaks 3 and 4) were also found by Hanusová et al. [40]. They assigned the higher binding energy peak to O-C=O, as has been done here, which is also consistent with the observation that the O 1s region found here contained a carboxylic acid environment.

The elements found for samples exposed to UV were fitted with peaks of the same number and approximate positions. For the extreme case of the sample exposed to 1344 h of UV radiation, the peak positions in comparison to 0 h are given in Table 4. The N 1s peak position did not change with UV exposure, nor did those of C Peak 2 (Peak 1 is set to 285.0 eV in order to calibrate the binding energy scale, and so by definition it does not change). Peaks A, B, 3, and 4 were slightly shifted to higher binding energies (smaller changes of 0.1 eV were considered to be within the precision of the instrument).

While the N 1s region did not change in position or shape upon UV exposure, the O 1s and C 1s regions did show differences between the 0 h and 1344 h exposed samples. As can be seen in Fig. 9, the intensity

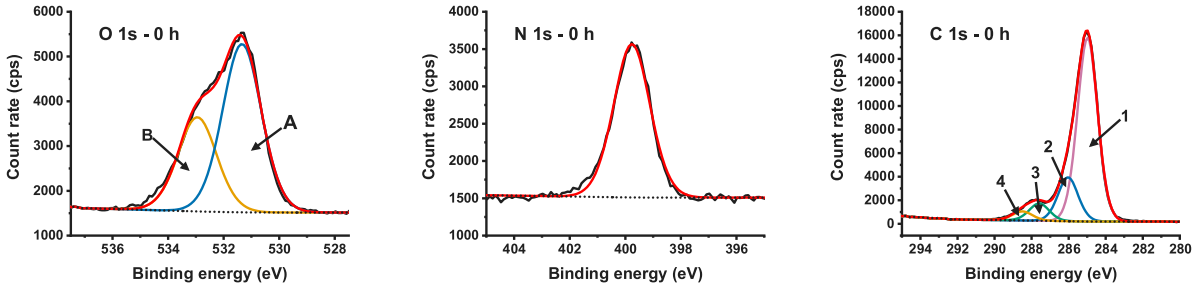

Fig. 7. High resolution XPS scans of the (a) O 1s, (b) N 1s, and (c) C 1s environments in a polyamide 12 sample that had not been subjected to UV weathering. The fitted peaks are assigned in Table 3.

Table 4
XPS peak positions in the O 1s, N 1s, and C 1s environments of polyamide 12 samples after no UV exposure, and after 2 months of UV exposure.

Element	Peak	Binding energy/eV	
		0 hours	1344 hours
O	B	532.9	533.1
	A	531.3	531.7
N	n/a	399.8	399.9
C	4	288.5	289.0
	3	287.6	287.8
	2	286.0	286.1
	1	285.0	285.0

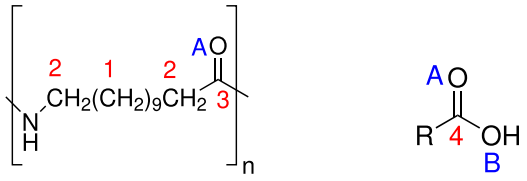

Fig. 8. Chemical formulae of the polyamide 12 polymer (a), and the carboxyl impurities inferred to be present from XPS data (b). The carbon and oxygen atoms are labelled to allow cross-reference with Table 3.

of O 1s Peak B increased relative to that of Peak A upon 1344 h of UV exposure, implying an increase in the relative concentration of carboxylic acid groups. Similarly, both the C 1s Peaks 3 and 4 increased in relative intensity with UV exposure, again suggesting an increase in the relative concentration of carboxyl groups.

Finally, the relative intensity of the O 1s region for each exposure time was quantified (Fig. 10). It can be seen that the surface O concentration increased continuously with UV exposure time, from around 11 At% at short exposure times, to 15.8 At% after 1344 h of exposure. The increase in relative concentration of O appears to be directly proportional to exposure time.

In summary, XPS data demonstrated an increase in the surface concentration of oxygen in the polyamide 12 samples upon UV exposure. Changes in peak shape in the O 1s and C 1s regions suggest that this increase was due to oxidation of the material to form new carbonyl groups, speculated to be carboxylic acids. This was consistent with the observation in Section 3.2 of increased UV absorbance by the samples with increasing exposure time. The increase in the concentration of these species appears to be directly proportional to exposure time, suggesting they are generated at a constant rate under irradiation of UV of constant intensity. While this has been shown to be the case up to two months of UV exposure, there is no reason not to expect these reactions to continue at the same rate beyond two months until every relevant reactant has been used up.

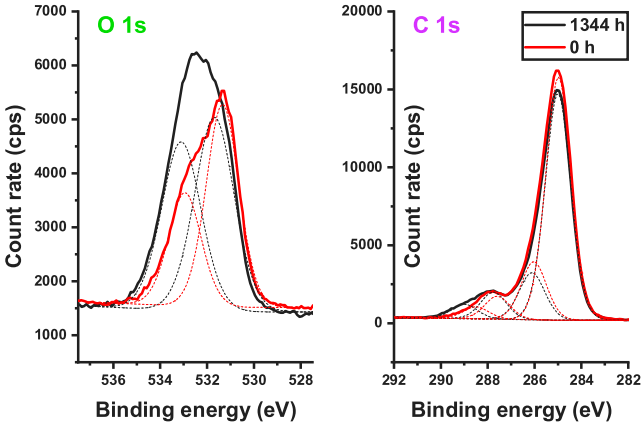

Fig. 9. A comparison of the O 1s and C 1s XPS environments in polyamide 12 samples after no UV exposure, and after 1344 h of UV exposure. The intensities of peaks associated with carboxyl species increase in both environments upon UV exposure.

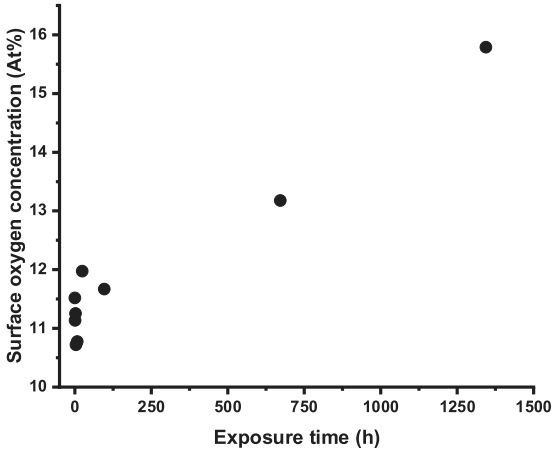

Fig. 10. Surface oxygen concentration of polyamide 12 samples versus UV exposure time. The oxygen content appears to increase at a constant rate as UV irradiation proceeds.

3.4. Mechanical properties

In order to determine if exposure to UV radiation affected the mechanical performance of Laser Sintered polyamide 12 parts in addition to altering their aesthetic and chemical properties, tensile testing was conducted. Fig. 11 demonstrates how the parts behaved under tensile load, with samples exposed to 168 h of UV irradiance or less all undergoing plastic deformation and “necking” prior to fracture. However, samples exposed to UV radiation for longer periods of time

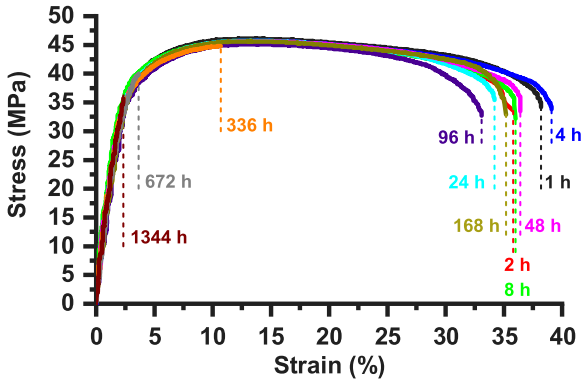

Fig. 11. Stress–strain curves for a single sample at each UV exposure time. Vertical dashed drop lines are included to show the point of fracture and are labelled with respect to UV exposure time in hours. (0 h UV excluded due to measurement fault).

were found to behave in a much more brittle manner, with little to no elongation beyond the yield point. This is reflected in Fig. 12, with samples exposed for 336 h or longer recording significant decreases in elongation at break (EaB). Ultimate Tensile Strength (UTS) also began to decrease at 336 h, although no significant change in Young's modulus (YM) was observed over the range of exposure times tested.

Since Young's modulus remained constant while UTS and EaB decreased significantly, it is suggested that the reduction in part integrity was a result of the increased ease with which cracks could form and propagate from the part surface at increased UV exposure times. That is to say, while a decrease in Young's modulus would require a change in behaviour throughout the bulk of the material, an increased tendency for critical failure could be caused by larger flaws or easier crack propagation anywhere in the material.

As the onset of discolouration occurred at a shorter exposure time than the onset of tensile property decrease, it was concluded that part's aesthetic properties were more sensitive to UV exposure than mechanical performance. While discolouration could be directly linked to chemical changes in the material as shown in Sections 3.2 and 3.3, the link between changing chemistry and deteriorating mechanical performance was less obvious. Given the changes in tensile properties with exposure to UV indicated a change of behaviour localised to the part surface, a closer examination of surface structure offered a potential route for further investigation.

3.5. Mono energetic positron spectroscopy (MEPS)

Potential changes in the nanoscale structure at the surfaces of UV weathered LS polyamide 12 parts were investigated using Mono-energetic Positron Spectroscopy (MePS). Changes were identified by measuring differences in the "free volume" between polymer chains, which are reported here in terms of Free Volume (average sizes of free volume voids) and Fractional Free Volume (an indication of the total free volume in a material). Free volume properties were measured as a function of implantation energy, and therefore depth, for all UV exposure times.

Fig. 13 shows three depth profiles for parts exposed to 0, 672 and 1344 h of UV radiation. In general, the shape of the free volume profiles were similar for each exposure time tested. This was also true for fractional free volume, suggesting that the nanoscale structure does not change as a function of depth due to UV exposure, but rather the variations are a characteristic of the parts in general. The results also indicated that changes to the nanoscale structure due to UV irradiation were present in the material down to a depth of at least 1.2 μm.

Whilst there were no apparent changes to the free volume and fractional free volume depth profiles, Fig. 13 shows a clear decrease in both FV and FFV at longer exposure times. This can also be seen in Fig. 14, where free volume and fractional free volume were plotted as a function of UV exposure time for five positron implantation energies (other energies are omitted for clarity). While both FV and FFV were relatively constant up to 168 h, beyond this point values began to decrease appreciably and continued to do so as exposure time was increased further. All of these results indicate that UV exposure promotes changes in the nanoscale structure at the part surface of LS polyamide 12 parts.

In order to determine if changes in free volume were linked to the decrease in mechanical performance reported previously, the two data sets were compared. Fig. 15 shows the mechanical (UTS and EaB) and the free volume properties averaged across all implantation energies (FV_{AV} and FFV_{AV}), as a function of UV exposure time. Both mechanical and free volume properties were found to remain fairly consistent up to 336 h of exposure (blue dashed line). Past this point, decreases in all four properties became appreciable. As the onset of both mechanical and free volume property reductions occurred at similar exposure times and decreased in a similar manner, it is reasonable to suggest that they are correlated. That is to say, prolonged UV exposure of polyamide 12 parts caused a continuous decrease in free volume, in turn causing a continuous decrease in part strength and ductility. This was suggested to be due to a reduction in polymer mobility near the part surfaces, permitting easier crack propagation. As the proposed decrease in polymer chain mobility resulting from decreasing free volume could be explained by either an increase in crystallinity or other change to the crystalline structure, further investigation into the polymer's structure in the crystalline region was conducted.

3.6. Differential Scanning Calorimetry

DSC was performed on samples at different UV exposure times in order to identify any changes in crystallinity and/or crystal structure at the part surface. As UV weathering was expected to only affect the outer regions of the parts, measurement from the bulks of samples were also carried out to confirm any changes in crystalline structure were limited to the surface. Example DSC traces for samples taken at different exposure times are shown in Fig. 16.

Both the bulk and surface samples at 0 hours of UV exposure show two melt peaks at approximately 179 °C (Peak 1) and 187 °C (Peak 2). The smaller, higher temperature peak was identified as the melting transition of virgin polyamide 12 powder, and, when seen in LS parts, represents particle cores which did not fully melt during sintering [41]. Polyamide 12 can adopt four different crystalline polymorphs which can coexist within the same polymer sample, and which can be converted between one another under different temperature, pressure, shearing, and solvent conditions [42–46]. These crystal polymorphs are differentiated by their distribution of hydrogen bonding both between adjacent polymer chains and between the lamellar sheets formed by collections of chains [44,47]. While detailed structural characterisation techniques such as X-ray scattering [42,45] and/or carbon NMR spectroscopy [45] would be required to allow precise determination of the natures and relative quantities of the polymorphs present in a given polyamide 12 sample, the two melt peaks seen in DSC of LS polyamide 12 parts are usually interpreted on their own to represent two forms of the polyamide 12 γ polymorph [41]. This is the most stable polymorph, and is the structure formed upon melting and recrystallisation of polyamide 12 under ambient pressure [43], as occurs during LS.

As can be seen in Fig. 16, although the bulk crystalline behaviour appeared to remain constant, several changes in the crystalline behaviour of the polyamide 12 surfaces occurred as UV ageing advanced. Firstly, Peak 1 and Peak 2 became increasingly poorly resolved, until the Peak 2 appeared to disappear completely. By 1344 hours of UV exposure, a new melt transition (Peak 3) appeared on the lower temperature shoulder of Peak 1 at approximately 169 °C. The emergence of Peak 3 at this temperature is consistent with the formation of the α polymorph of polyamide 12 [46]. In general, the α polyamide 12

polymorph can only be obtained under certain conditions, for example by casting from specific solutions, or by crystallisation at high pressure [43]. However, the chemical changes induced by UV irradiation also appear to result in significant transformations of the polyamide 12 crystalline structure, apparently causing interconversion of the γ forms, and eventually resulting in conversion from the γ polymorph into the α polymorph. While it is difficult to determine the exact mechanisms which could cause this behaviour, it is speculated to be related to changes in the distribution of hydrogen bonding within the polymer, for example by the introduction of the new carboxyl groups seen in Section 3.3.

In addition to changes to the secondary peaks, UV exposure also caused a continuous decrease in the temperature of the main γ peak (Peak 1), as shown in Fig. 17a. Specifically, the peak melt temperature for the surface samples reduced from (179.6 ± 0.2) °C initially to (177.7 ± 0.8) °C after 1344 hours of exposure. In contrast, the peak melt temperature in the bulk remained roughly constant. Such a decrease in melt temperature at the part surface suggests the introduction of impurities into the polyamide 12 that disrupt the crystalline structure, which is consistent with the generation of new photo-oxidation products within the polymer. As shown in Fig. 17b, UV ageing was also associated with an increase in the melt enthalpy of the polyamide 12, which rose from (58 ± 2) Jg^{-1} for unexposed polyamide 12, to (65 ± 1) Jg^{-1} after 1344 hours of UV exposure. This suggests an increase in the total crystallinity of the surface regions of the polymer parts as UV ageing proceeds. Once again however, no trend in melt enthalpy versus UV exposure time was seen in the bulk. The increase in melt enthalpy at the surface was speculated to be due to the increased tendency towards hydrogen bonding caused by the generation of new oxygen-bearing functional groups on the polymer, such as carboxylic acids. Similar trends in melt temperature and melt enthalpy were seen by Yano and Murayama for UV-irradiated polyamide 6 [18].

Overall, the DSC results demonstrate that UV irradiation caused significant changes in the type and extent of crystallinity at the surfaces of LS polyamide 12 parts. These changes were most likely a result of the introduction of new oxygen-bearing functional groups to the polymer as a consequence of photo-oxidation, such as the carboxyl groups identified in Section 3.3. Such functional groups would be expected to participate in hydrogen bonding, and it is proposed that their random introduction into the polymer chains increased the extent of interchain hydrogen bonding interactions in a way that increases the size or number of crystalline domains, whilst simultaneously disrupting the preexisting crystalline order. Regardless of the exact mechanism by which UV weathering changed the crystalline structure of the part surfaces, it is reasonable to conclude that these changes are the cause of the reduction in free volume in the polymer seen in Section 3.5 and subsequent deterioration in part strength and ductility seen in Section 3.4.

4. Conclusions

In summary, Laser Sintered polyamide 12 parts were subjected to up to two months of constant UV irradiation. Colour measurements showed that the parts became measurably more yellow after 24 h of irradiation, and discolouration, quantified in terms of a decreasing reflected intensity of blue light, was exacerbated with increased UV

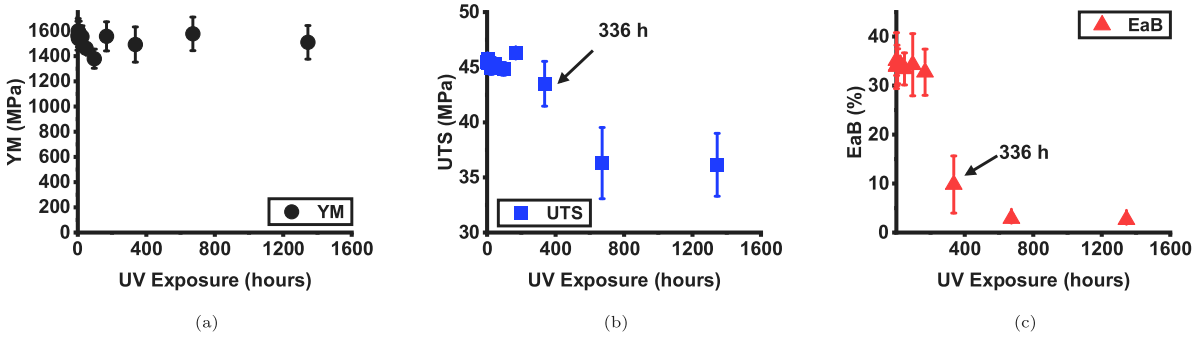

Fig. 12. The mechanical properties of LS parts as a function of UV exposure time determined by tensile testing. Whilst Young's modulus remains constant, both Ultimate Tensile Strength and Elongation at break decreased after 336 h of exposure. The standard error of 4 samples is represented by solid bars.

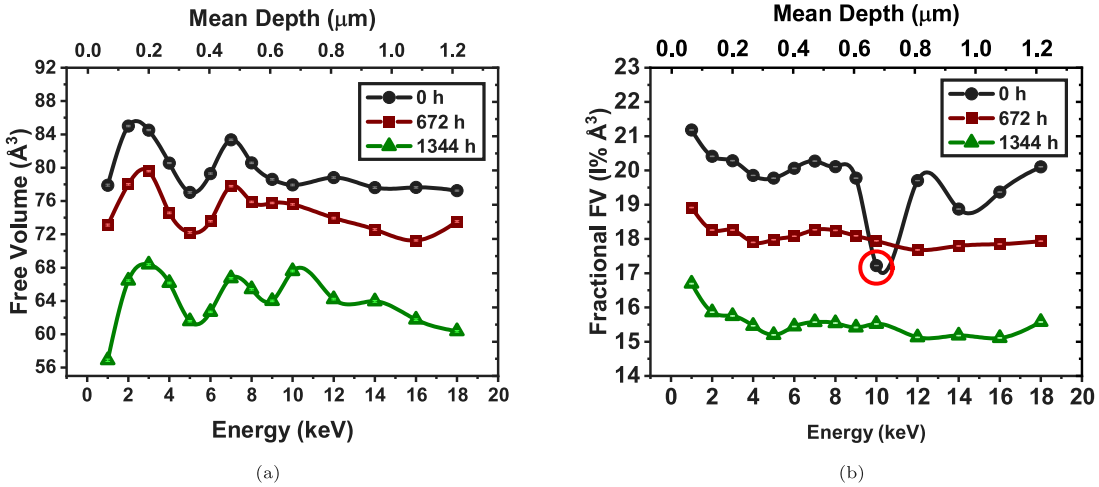

Fig. 13. The free volume (FV) and fractional free volume (FFV) as a function of implantation energy/depth measured by MEPS. Solid lines connecting data are included as a guide for the reader. A red circle highlights an anomaly in fractional free volume. Fitting errors are represented by solid bars but are smaller than the data point size. (For interpretation of the references to colour in this figure legend, the reader is referred to the web version of this article.)

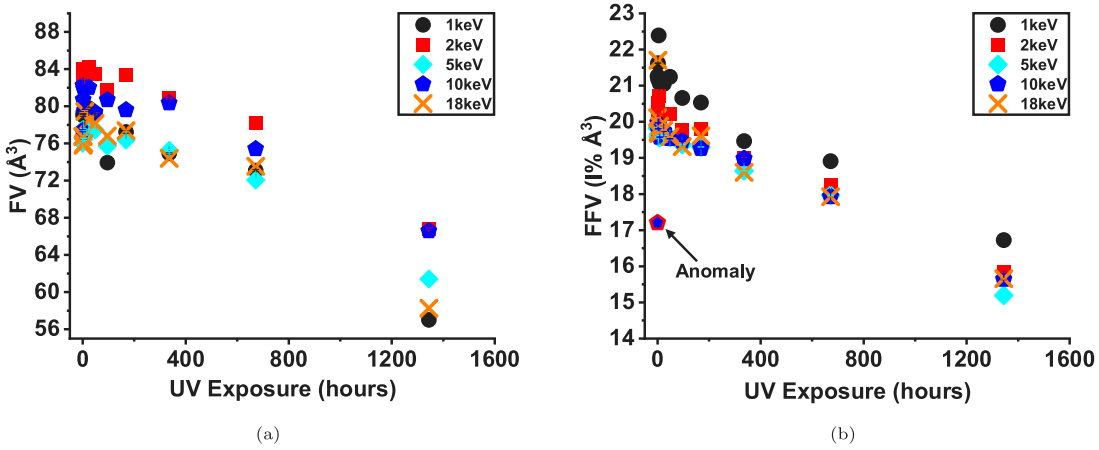

Fig. 14. The free volume (FV) and fractional free volume (FFV) as a function of UV exposure time for five different positron implantation energies. Errors from fitting lifetime data are shown but are not visible due to their small size. An anomaly for the FFV 10 keV data series is shown by an arrow.

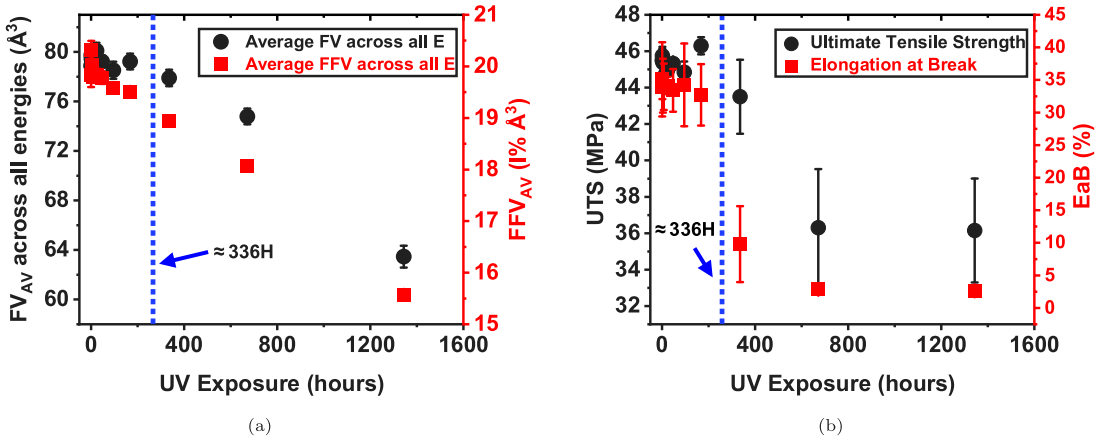

Fig. 15. The (a) free volume & fractional free volume averaged across all implantation energies (FV_{AV} & FFV_{AV}) alongside the (b) ultimate tensile strength (UTS) & elongation at break (EaB) as a function of UV exposure time. The time at which there is a decrease in properties is indicated by blue dashed lines. The standard error is represented by solid bars. (For interpretation of the references to colour in this figure legend, the reader is referred to the web version of this article.)

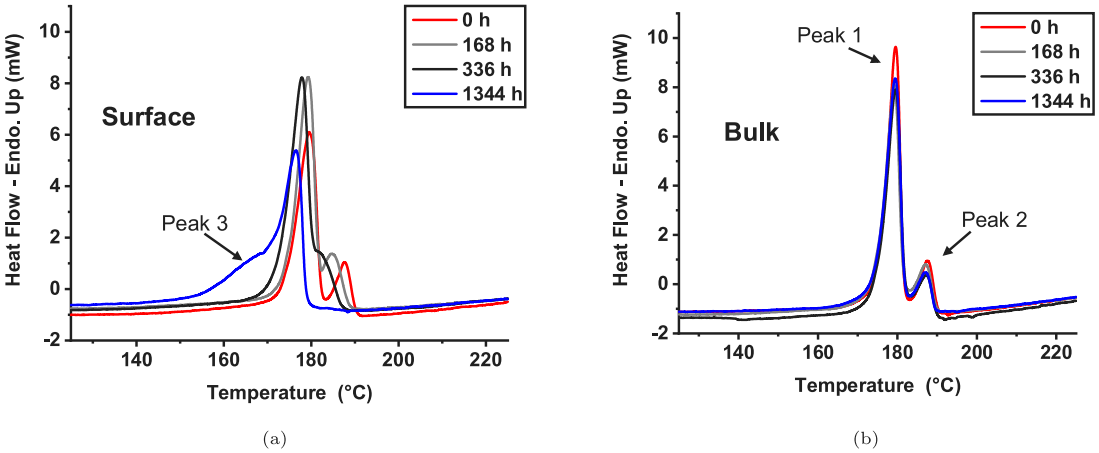

Fig. 16. DSC traces of samples taken from the (a) surface or (b) bulk of UV-exposed LS polyamide 12 parts. Significant changes to the crystalline behaviour of the surface samples are apparent, but the bulk samples remain similar regardless of UV exposure time.

exposure. Reflectance spectroscopy over UV and visible wavelengths confirmed increased absorbance of blue wavelengths by the parts at long exposure times, and also demonstrated a positive correlation between UV absorbance by the parts and UV irradiation time. It was suggested that the increasing UV absorbance was due to an increasing concentration of carbonyl groups in the part surfaces. This was subsequently supported by XPS results which demonstrated that surface oxygen concentration in the parts was proportional to UV exposure time, and identified changes in the O 1s and C 1s environments at

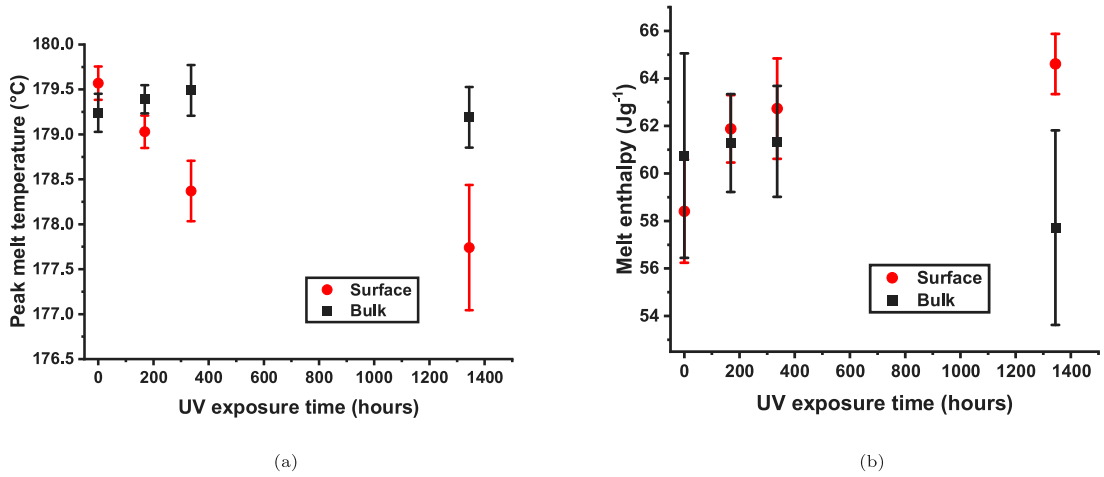

Fig. 17. (a) Peak melt temperature (γ polymorph) and (b) melt enthalpy versus UV exposure time for samples taken from the surface and bulk of LS polyamide 12 parts. For the surface samples, melt temperature decreases and melt enthalpy increases as UV ageing proceeds. In contrast, these properties stay approximately constant for the bulk samples. The error bars are the standard deviation of four measurements.

long exposure times which were consistent with the generation of new carboxylic acid groups.

Chemical changes in the parts following UV exposure were accompanied by a significant decrease in their mechanical performance. More specifically, while the Young's modulus did not change upon UV irradiation, parts became substantially more brittle, evidenced by significant decreases in both UTS and EaB. The observation that the Young's modulus was unaffected by UV exposure while strength and ductility decreased was consistent with UV exposure only causing degradation at the part surface, as only a small region of a sample need contain larger flaws or be more susceptible to crack propagation for critical failure to occur at lower loads.

The changes in mechanical properties were suspected to be linked to structural changes within the material. MePS investigations demonstrated that the observed decrease in mechanical properties correlated to a drop in free volume at the part surfaces (down to a depth of at least 1.2 microns). It was therefore concluded that the increase in part brittleness was caused by a reduction in polymer mobility in the surface region. Subsequent DSC measurements implied that significant changes in crystal structure within the polyamide 12 surfaces had taken place during the course of UV ageing. These included changes in relative DSC peak intensities of the polyamide 12 polymorphs present, a decrease in peak melt temperature of approximately 1.9 °C, and an approximately 7 Jg^{-1} increase in melt enthalpy. The evolution of the polymer crystal structure was consistent with the chemical changes observed upon UV irradiation, which were expected to change the extent and distribution of hydrogen bonding within the material. This was concluded to be the cause of the decreased free volume and reduced polymer mobility within the surfaces of the UV-exposed parts, and subsequently the cause of the decreases in part strength and ductility.

Overall, it can be concluded that environmental UV radiation presents a serious concern for the use of Laser Sintered polyamide 12 parts in outdoor applications. More specifically, several years of exposure to natural UV would be expected to lead to extensive discolouration of such parts, as well as a significant drop in their mechanical properties. Without steps taken to mitigate these effects, Laser Sintered polyamide 12 parts are concluded to be unsuitable for long-term outdoor applications in which they would be required to remain aesthetically pleasing and/or structurally robust. This would make them unsuitable for use as external automotive parts, as suggested in Section 1.

There are several possible avenues for future research into this area. Firstly, it should be determined exactly what structural changes are occurring to reduce surface free volume in polyamide 12 upon UV irradiation. As an example, X-ray scattering measurements should allow determination of any changes in crystallinity that are not decipherable by DSC (for example, crystallite size). Similarly, bulk PALS measurements would complement the MePS studies of the part surfaces, as this would confirm whether the decreases in part free volume are indeed isolated to the surface region. Work should then be carried out to identify ways to mitigate the effect of UV irradiation on the polyamide 12 parts. This could include the addition of UV-blockers, such as TiO_2, or antioxidants to the polymer or powder before manufacture. Importantly, it would need to be demonstrated that such additives can be incorporated into the polymer powder without reducing processability or final part properties. Alternatively, a protective coating could be developed to be applied to the parts during post-processing. However, an additional step such as this might prove to add undesirable cost or complexity to the manufacturing process. Regardless of the final approach adopted, it is clear that UV weathering must be mitigated against before polyamide 12 parts can be used for long-term, outdoor applications, such as external automotive components. UV's effect on other materials which can be processed in Laser Sintering should also be investigated.

In addition to further investigation into the effects of UV on polyamide 12 parts, other environmental factors should also be explored such as wind, humidity and temperature, including combinations of these conditions. One particularly interesting avenue to pursue could be the impact of surface embrittlement due to UV exposure on abrasive wear from wind-carried particles.

CRediT authorship contribution statement

Alec S.D. Shackleford: Conceptualization, Methodology, Formal analysis, Investigation, Writing - original draft, Writing - review & editing, Visualization, Project administration. **Rhys J. Williams:** Formal analysis, Investigation, Writing - original draft, Writing - review & editing, Visualization. **Ryan Brown:** Formal analysis, Investigation, Writing - original draft, Writing - review & editing. **James R. Wingham:** Formal Analysis, Investigation, Writing - original draft, Writing - review & editing. **Candice Majewski:** Conceptualization, Methodology, Writing - review & editing, Supervision.

Declaration of competing interest

The authors declare that they have no known competing financial interests or personal relationships that could have appeared to influence the work reported in this paper.

Acknowledgements

The authors would like to thank Dr. Oskar Liedke at the HZDR for MePS advice and access. UV/visible spectra were collected by Dr. Andrew Parnell. XPS data was collected by Dr. Deborah Hammond at the Sheffield Surface Analysis Centre. Laser Sintered parts were manufactured by Wendy Birtwistle.

Funding

This work was supported by the MAPP Manufacturing Hub, UK [EP/P006566/1] and University of Sheffield Impact Acceleration Account 2017–2020, UK [EP/R511754/1].

References

[1] Wohlers Report 2020, Wohlers Associates, 2020.
[2] B.S. Ian Gibson, David.W. Rosen, B. Stucker, Additive Manufacturing Technologies: Rapid Prototyping to Direct Digital Manufacturing, Springer, 2010, p. 11.
[3] C.L.C.K. Chua, K.F. Leong, C. Lim, Rapid Prototyping: Principles and Applications, World Scientific, 2003, p. 17.
[4] P.D.N. Hopkinson, R.J.M. Hague, P.M. Dickens, Rapid Manufacturing: An Industrial Revolution for the Digital Age, Wiley, 2006, p. 64.
[5] R.D. Turner, J.R. Wingham, T.E. Paterson, J. Shepherd, C. Majewski, Use of silver-based additives for the development of antibacterial functionality in Laser Sintered polyamide 12 parts, Sci. Rep. 10 (2020) 892, http://dx.doi.org/10.1038/s41598-020-57686-4.
[6] I. Gibson, D. Shi, Material properties and fabrication parameters in selective laser sintering process, Rapid Prototyp. J. 3 (4) (1997) 129–136, http://dx.doi.org/10.1108/13552549710191836.
[7] B. Caulfield, P.E. McHugh, S. Lohfeld, Dependence of mechanical properties of polyamide components on build parameters in the SLS process, J. Mater Process. Technol. 182 (1–3) (2007) 477–488, http://dx.doi.org/10.1016/j.jmatprotec.2006.09.007.
[8] T.L. Starr, T.J. Gornet, J.S. Usher, The effect of process conditions on mechanical properties of laser-sintered nylon, Rapid Prototyp. J. 17 (6) (2011) 418–423, http://dx.doi.org/10.1108/13552541111184143.
[9] C. Gayer, J. Abert, M. Bullemer, S. Grom, L. Jauer, W. Meiners, F. Reinauer, M. Vučak, K. Wissenbach, R. Poprawe, J.H. Schleifenbaum, H. Fischer, Influence of the material properties of a poly(D,L-lactide)/β-tricalcium phosphate composite on the processability by selective laser sintering, J. Mech. Behav. Biomed. Mater. 87 (2018) 267–278, http://dx.doi.org/10.1016/j.jmbbm.2018.07.021.
[10] S.C. Ligon, R. Liska, J. Stampfl, M. Gurr, R. Mülhaupt, Polymers for 3D printing and customized additive manufacturing, Chem. Rev. 117 (15) (2017) 10212–10290, http://dx.doi.org/10.1021/acs.chemrev.7b00074.
[11] M. Vasquez, B. Haworth, N. Hopkinson, Optimum sintering region for laser sintered Nylon-12, Proc. Inst. Mech. Eng. B 225 (12) (2011) 2240–2248, http://dx.doi.org/10.1177/0954405411414994.
[12] G. Wypych, Handbook of Polymers, second ed., ChemTech Publishing, 2016, p. 249.
[13] Plastics News, BMW sees potential of 3D printing in new business models, 2020, (Accessed: 11 november 2020).
[14] T.C.T. Magazine, Ford to explore using stratasys infinite build 3D printer to produce large scale automotive components, 2020, (Accessed: 11 november 2020).
[15] B. Rånby, Photodegradation and photo-oxidation of synthetic polymers, J. Anal. Appl. Pyrol. 15 (C) (1989) 237–247, http://dx.doi.org/10.1016/0165-2370(89)85037-5.
[16] N.S. Allen, Thermal and photo-chemical oxidation of nylon 6,6: Some aspects of the importance of α,β-unsaturated carbonyl groups and hydroperoxides, Polym. Degrad. Stab. 8 (1) (1984) 55–62, http://dx.doi.org/10.1016/0141-3910(84)90071-5.
[17] S. Carroccio, C. Puglisi, G. Montaudo, MALDI investigation of the photooxidation of nylon-66, Macromolecules 37 (16) (2004) 6037–6049, http://dx.doi.org/10.1021/ma049521n.
[18] S. Yano, M. Murayama, Photo-oxidation of nylon 6 above 300 nm, Polym. Photochem. 1 (3) (1981) 177–190, http://dx.doi.org/10.1016/0144-2880(81)90018-X.
[19] P.N. Thanki, C. Ramesh, R.P. Singh, Photo-irradiation induced morphological changes in nylon 66, Polymer 42 (2) (2001) 535–538, http://dx.doi.org/10.1016/S0032-3861(00)00374-8.
[20] Y. Fujiwara, S.H. Zeronian, Formation of cracks on photodegraded nylon 6 filaments, J. Appl. Polym. Sci. 27 (8) (1982) 2773–2782, http://dx.doi.org/10.1002/app.1982.070270803.
[21] M. Moezzi, J. Yekrang, M. Ghane, M. Hatami, The effects of UV degradation on the physical, thermal, and morphological properties of industrial nylon 66 conveyor belt fabrics, J. Ind. Text. 50 (2) (2020) 240–260, http://dx.doi.org/10.1177/1528083718825316.
[22] R. Shamey, K. Sinha, A review of degradation of nylon 6. 6 as a result of exposure to environmental conditions, Rev. Prog. Color. Relat. Top. 33 (1) (2003) 93–107, http://dx.doi.org/10.1111/j.1478-4408.2003.tb00147.x.
[23] A. Pilipović, M. Rujnić-Sokele, M. Šercer, Impact of ageing, different share of recycled material and orientation on SLS polyamide product hardness, AIP Conf. Proc. 1779 (1) (2016) 100001, http://dx.doi.org/10.1063/1.4965569.
[24] R. Goodridge, R. Hague, C. Tuck, Effect of long-term ageing on the tensile properties of a polyamide 12 laser sintering material, Polym. Test. 29 (4) (2010) 483–493, http://dx.doi.org/10.1016/j.polymertesting.2010.02.009.
[25] D.W. Gidley, H.-G. Peng, R.S. Vallery, Positron annihilation as a method to characterize porous materials, Annu. Rev. Mater. Res. 36 (1) (2006) 49–79, http://dx.doi.org/10.1146/annurev.matsci.36.111904.135144.
[26] C. He, T. Suzuki, E. Hamada, H. Kobayashi, K. Kondo, V.P. Shantarovich, Y. Ito, Characterization of polymer films using a slow positron beam, Mater. Res. Innov. 7 (1) (2003) 37–41, http://dx.doi.org/10.1080/14328917.2003.11784757.
[27] C. Arlett, B. Bridges, A. Brøgger, B.L. Diffey, J.M. Elwood, E.E. A, D. English, P.D. Forbes, R.P. Gallagher, J.W. Grisha, IARC Monographs on the Evaluation of Carcinogenic Risks to Humans - Solar and Ultraviolet Radiation, 1992, p. 52.
[28] Delft Research Team, The Delft Intense Slow Positron Beam 2D-ACAR Facility for Analysis of Nanocavities and Quantum Dots (Ph.D. thesis), ISBN: 9040723370, 2002.
[29] N. Nath Mondal, Development of slow positron beam lines and applications, AIP Conf. Proc. 1970 (1) (2018) http://dx.doi.org/10.1063/1.5040217.
[30] A. Wagner, W. Anwand, A.G. Attallah, G. Dornberg, M. Elsayed, D. Enke, A.E.M. Hussein, R. Krause-Rehberg, M.O. Liedke, K. Potzger, T.T. Trinh, Positron annihilation lifetime spectroscopy at a superconducting electron accelerator, J. Phys. Conf. Ser. 791 (1) (2017) 012004, http://dx.doi.org/10.1088/1742-6596/791/1/012004.
[31] A. Wagner, M. Butterling, M.O. Liedke, K. Potzger, R. Krause-Rehberg, Positron annihilation lifetime and Doppler broadening spectroscopy at the ELBE facility, AIP Conf. Proc. 1970 (2018) 040003, http://dx.doi.org/10.1063/1.5040215.
[32] R. Alcaraz de la Osa, I. Iparragirre, D. Ortiz, J.M. Saiz, The extended Kubelka–Munk theory and its application to spectroscopy, ChemTexts 6 (1) (2020) 1–14, http://dx.doi.org/10.1007/s40828-019-0097-0.
[33] A.S. Jääskeläinen, T. Liitiä, UV/vis reflectance spectroscopy reveals the changes in fibre chemistry during ageing, Spectrosc. Eur. 19 (5) (2007) 11–13, URL https://www.spectroscopyeurope.com/article/uvvis-reflectance-spectroscopy-reveals-changes-fibre-chemistry-during-ageing.
[34] R.D. Martinez, A.A. Buitrago, N.W. Howell, C.H. Hearn, J.A. Joens, The near U.V. absorption spectra of several aliphatic aldehydes and ketones at 300 K, Atmos. Environ. A 26 (5) (1992) 785–792, http://dx.doi.org/10.1016/0960-1686(92)90238-G.
[35] G. Ruderman, E.R. Caffarena, I.G. Mogilner, E.J. Tolosa, Hydrogen bonding of carboxylic acids in aqueous solutions - UV spectroscopy, viscosity, and molecular simulation of acetic acid, J. Solut. Chem. 27 (10) (1998) 935–948, http://dx.doi.org/10.1023/A:1022615329598.
[36] N.S. Allen, A. Parkinson, Ultraviolet derivative absorption spectra of nylon 6,6: Effect of photolysis versus photo-induced oxidation, Polym. Degrad. Stab. 4 (4) (1982) 239–244, http://dx.doi.org/10.1016/0141-3910(82)90047-7.
[37] P. Louette, F. Bodino, J.-J. Pireaux, Nylon 6 (N6) reference XPS reference core level and energy loss spectra, Surf. Sci. Spectra 12 (1) (2005) 12–17, http://dx.doi.org/10.1116/11.20050903.
[38] D. Briggs, G. Beamson, XPS studies of the oxygen 1s and 2s levels in a wide range of functional polymers, Anal. Chem. 65 (11) (1993) 1517–1523, http://dx.doi.org/10.1021/ac00059a006.
[39] B. Scherer, I.L. Kottenstedde, F.M. Matysik, Material characterization of polyamide 12 and related agents used in the multi jet fusion process : complementary application of high resolution mass spectrometry and other advanced instrumental techniques, Mon. Chem.- Chem. Monthly 151 (8) (2020) 1203–1215, http://dx.doi.org/10.1007/s00706-020-02646-x.
[40] J. Hanusová, D. Kováčik, M. Stupavská, M. Černák, I. Novák, Atmospheric pressure plasma treatment of polyamide-12 foils, Open Chem. 13 (1) (2015) 382–388, http://dx.doi.org/10.1515/chem-2015-0049.
[41] H. Zarringhalam, N. Hopkinson, N.F. Kamperman, J.J. de Vlieger, Effects of processing on microstructure and properties of SLS Nylon 12, Mater. Sci. Eng. A 435–436 (2006) 172–180, http://dx.doi.org/10.1016/j.eurpolymj.2017.05.01410.1016/j.msea.2006.07.084.
[42] L. Li, M.H. Koch, W.H. De Jeu, Crystalline structure and morphology in nylon-12: A small- and wide-angle X-ray scattering study, Macromolecules 36 (5) (2003) 1626–1632, http://dx.doi.org/10.1016/j.eurpolymj.2017.05.01410.1021/ma025732l.
[43] N. Hiramatsu, K. Haraguchi, S. Hirakawa, Study of transformations among α, γ and γ' forms in Nylon 12 by X-Ray and DSC, Japan. J. Appl. Phys. 22 (Part 1, No. 2) (1983) 335–339, http://dx.doi.org/10.1143/jjap.22.335.

[44] B. de Jager, T. Moxham, C. Besnard, E. Salvati, J. Chen, I.P. Dolbnya, A.M. Korsunsky, Synchrotron x-ray scattering analysis of nylon-12 crystallisation variation depending on 3D printing conditions, Polymers 12 (5) (2020) http://dx.doi.org/10.3390/POLYM12051169.

[45] N. Dencheva, T.G. Nunes, M. Jovita Oliveira, Z. Denchev, Crystalline structure of polyamide 12 as revealed by solid-state 13C NMR and synchrotron WAXS and SAXS, J. Polym. Sci. B 43 (24) (2005) 3720–3733, http://dx.doi.org/10.1002/polb.20672.

[46] T. Ishikawa, S. Nagai, N. Kasai, Thermal behavior of α nylon-12, J. Polym. Sci.: Polym. Phys. Ed. 18 (6) (1980) 1413–1419, http://dx.doi.org/10.1002/pol.1980.180180619.

[47] S. Dasgupta, W.B. Hammond, W.A. Goddard, Crystal structures and properties of nylon polymers from theory, J. Am. Chem. Soc. 118 (49) (1996) 12291–12301, http://dx.doi.org/10.1021/ja944125d.